

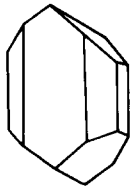
## Water-deficient mylonite zones — An example from the Pyrenees

CEES W. PASSCHIER

*Instituut voor Aardwetenschappen, Budapestlaan 4, 3508 TA Utrecht (The Netherlands)*

### LITHOS

Passchier, C.W., 1985. Water-deficient mylonite zones — An example from the Pyrenees. *Lithos*, 18: 115–127.



Some mylonite zones which operate at retrograde conditions in metamorphic rocks have a low water content of the metamorphic fluid, resulting in an incomplete reequilibration of the mineral assemblages. Recognition of such zones is important for a correct assessment of *P-T* conditions of deformation, especially where these data are used for reconstructing palaeogeometry of exhumed normal fault and thrust zones. An example of a water-deficient mylonite zone from the Pyrenees is characterized by incomplete breakdown of sillimanite + orthoclase in the stability field of muscovite + quartz, pure- $\text{CO}_2$  fluid inclusions, limited postkinematic grain growth and high differential stresses during the deformation as indicated by recrystallized quartz grain size.

(Accepted after revision January 21, 1985)

### Introduction

Ductile deformation in mylonite zones commonly leads to pronounced changes in mineralogy and bulk chemistry of the zone compared to the parent rock (Burwash and Krupica, 1969; Beach, 1976; Mitra, 1978; Brodie, 1981). Such deformation-induced changes are usually attributed to enhanced migration of metamorphic fluids with a large aqueous component along the zones (Beach, 1976). Fluids with an aqueous component have the additional effect of hydrolytic weakening of quartz (Tullis and Yund, 1980) and possibly of other minerals.

Many low-grade mylonite zones show evidence of enhanced retrograde metamorphic reactions compared to the undeformed surrounding parent rock in which relatively high-grade mineral assemblages have been preserved. This can be attributed to uplift and cooling of the parent rock before mylonite generation and preferential re-equilibration of relic mineral assemblages in the deforming zone due to the influx of aqueous fluids and enhanced diffusion (Beach, 1976; White et al., 1980). If the metamorphic fluid in a mylonite zone would have a low aqueous component for whatever reason,

retrogression and hydrolytic weakening could be expected to be of lesser importance. Since estimations of the metamorphic conditions of mylonitic deformation are usually based on stable mineral assemblages in the deformed rock, this could lead to serious errors. This problem is especially serious where mylonite fabrics are used to assess a geothermal gradient or depth of decollement in exhumed normal fault or thrust systems. Detailed analysis of the fabric and large-scale geometry of mylonite zones which formed under water-deficient conditions could produce simple criteria for their recognition. A major shear zone in the Saint-Barthélemy Massif, French Pyrenees, is treated as an example.

### Regional geology

The Saint-Barthélemy Massif, one of the northern Pyrenean Massifs in France consists of a gneiss core, covered by metasediments of Palaeozoic age (Passchier, 1982a, b). In the gneiss core, basal granulite facies gneiss of probable Proterozoic age is overlain by peraluminous granodiorite which locally grades into migmatitic gneiss derived from the meta-

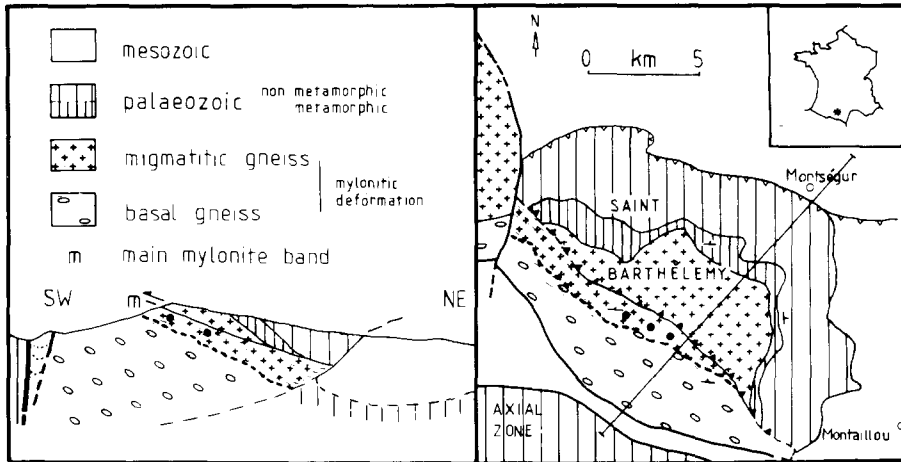


Fig. 1. Schematic map and cross-section of the Saint-Barthélemy Massif after Zwart (1954) and Passchier (1984c).

sediment cover (Fig. 1). The granodiorite and migmatitic gneiss are associated with amphibolite facies regional metamorphism of Variscan age (Passchier, 1982b; Vielzeuf, 1984).

A gently north-dipping 2 km thick mylonite zone transects the basal gneiss and the granodiorite. It is interpreted as a fragment of a major south-dipping low-angle normal shear zone of post-Variscan and pre-Eocene age, transected by low-angle Alpine thrust faults (Passchier, 1984c). North-directed thrusting on these faults brought the Saint-Barthélemy Massif on top of Mesozoic sediments of the Aquitaine basin, and tilted the normal shear zone into its present position (McCaig and Wickham, 1984; Passchier, 1984c).

Mylonitic fabric elements in the shear zone are progressively better developed from the basal gneiss upwards into the granodiorite, where a sharp ultramylonite contact separates mylonites from overlying undeformed granodiorite. This asymmetric distribution of fabric development in the shear zone is interpreted as an effect of the juxtaposition of relatively cool hanging wall rocks on hot footwall gneisses along this section of the active zone (mylonite-dominated footwall geometry; Passchier, 1984c).

#### Undeformed granodiorite

The undeformed granodiorite as exposed above the mylonite zone is medium grained and consists of randomly orientated quartz, oligoclase-andesine, micropertthitic orthoclase, hypidiomorphic biotite (up

to 20 vol.%) and muscovite (up to 5 vol.%), 1–2 mm long prismatic and fibrolitic sillimanite (up to 5 vol.%) and accessory ilmenite, apatite, zircon and monazite. Almandine and cordierite up to 2 mm in diameter are observed in some samples. Muscovite was the last mineral of the assemblage to develop.

#### Mylonitized granodiorite

The fabric of the mylonitized granodiorite consists of a complex alternation of porphyroclasts and lenses of different mineral composition which define a shape fabric with a planar ( $S_g$ ) and linear ( $L_g$ ) element (Fig. 2; Passchier, 1982a, 1984a). The follow-



Fig. 2. Microfabric of mylonitized granodiorite with alternating quartz ribbons ( $Q$ ), feldspar aggregates and lensoid biotite clasts ( $b$ ) which define the foliation. A weak shear band cleavage is developed from lower left to upper right.

ing elements are most common: (1) lens- or rod-shaped domains of plagioclase or orthoclase containing irregularly shaped porphyroclasts cut by micro-shear zones and mantled by fine-grained recrystallized feldspar; (2) lens- or rod-shaped domains of partially recrystallized quartz, commonly monocrystalline ribbons; (3) porphyroclasts of biotite or muscovite, either lozenge-shaped or equidimensional and strongly kinked or folded, some surrounded by fine-grained recrystallized mica. These elements are commonly separated by a dark, fine-grained (1–5  $\mu\text{m}$ ) matrix of biotite, plagioclase and quartz. The shape fabric is deflected around porphyroclasts of feldspar and almandine, up to 5 mm in diameter.

Finite strain distribution in mylonitized granodiorite is rather homogeneous on a metre-scale, without the anastomosing pattern of minor shear zones commonly observed in mylonitic terrains elsewhere (Ramsay and Allison, 1979; Simpson et al., 1982). Locally, a weak macroscopic shear band cleavage occurs, indicating dominant southward movement of the hanging wall (Fig. 2; Simpson and Schmid, 1983). This is confirmed by microscopic sense of shear markers such as lozenge-shaped micas, elongated new grains in quartz ribbons and displacement patterns on intracrystalline micro-shear zones (Passchier, 1983; Simpson and Schmid, 1983). These data combined with strain analysis of deformed xenoliths in the zone indicate that deformation proceeded by rotational non-coaxial flow with a consistent shear sense in most of the mylonite volume studied (Passchier, 1982b; Lister and Williams, 1983). Orientation patterns of mylonitic shape fabric elements are very constant over the area studied and have not been disturbed by later phases of deformation (Passchier, 1982b, 1984a).

## Deformation microstructure

### Quartz

Deformation of the originally equidimensional quartz grains resulted in flattened old grains with undulose extinction and equidimensional or elongated subgrains. Dynamic recrystallization was mainly by subgrain rotation at sites of high strain energy like grain mantles and intracrystalline shear zones (cf. White, 1976). Static grain growth was of minor importance in most samples. The new grains are

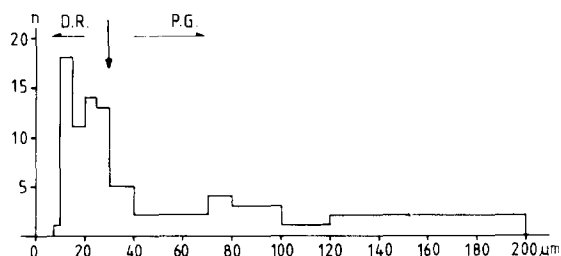


Fig. 3. Histogram of the size of dynamically recrystallized quartz grains and new grains affected by postkinematic growth. 134 points in 38 thin sections. *D.R.* – thin sections with dynamic recrystallization only. *P.G.* – thin sections with postkinematic grain growth.

usually equidimensional and of identical size to optical subgrains, ranging from 7 to 30  $\mu\text{m}$  over the samples studied (Fig. 3): in a thin section the variation in grain size is in the order of a few micrometres only (cf. Etheridge and Wilkie, 1981). Some samples contain new grains with a diameter exceeding 30  $\mu\text{m}$  (Fig. 3), but these always contain smaller optical subgrains and show signs of static grain growth. The presence of a strong crystallographic preferred orientation in recrystallized aggregates (Passchier, 1982b, 1983) indicates that grain boundary sliding was of limited significance in quartz aggregates (cf. Boullier and Gueguen, 1975).

### Quartz ribbons

Rod-shaped monocrystalline quartz ribbons (Marjoribanks, 1976; Bouchez, 1977) up to 1 mm

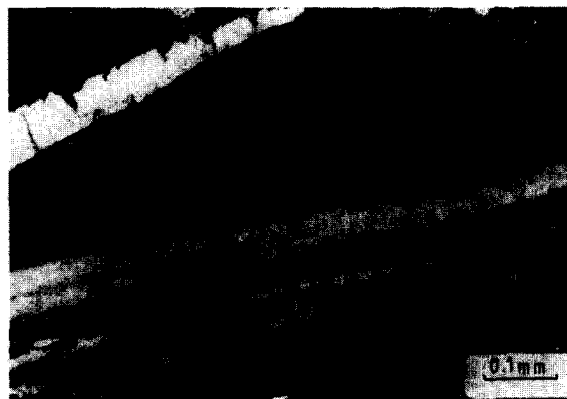


Fig. 4. Monocrystalline quartz ribbon, separated into domains with a distinct crystallographic preferred orientation by low- or high-angle boundaries, commonly lined with equidimensional new grains. Rutile needles (*r*) have been boudinaged. Crossed polars.

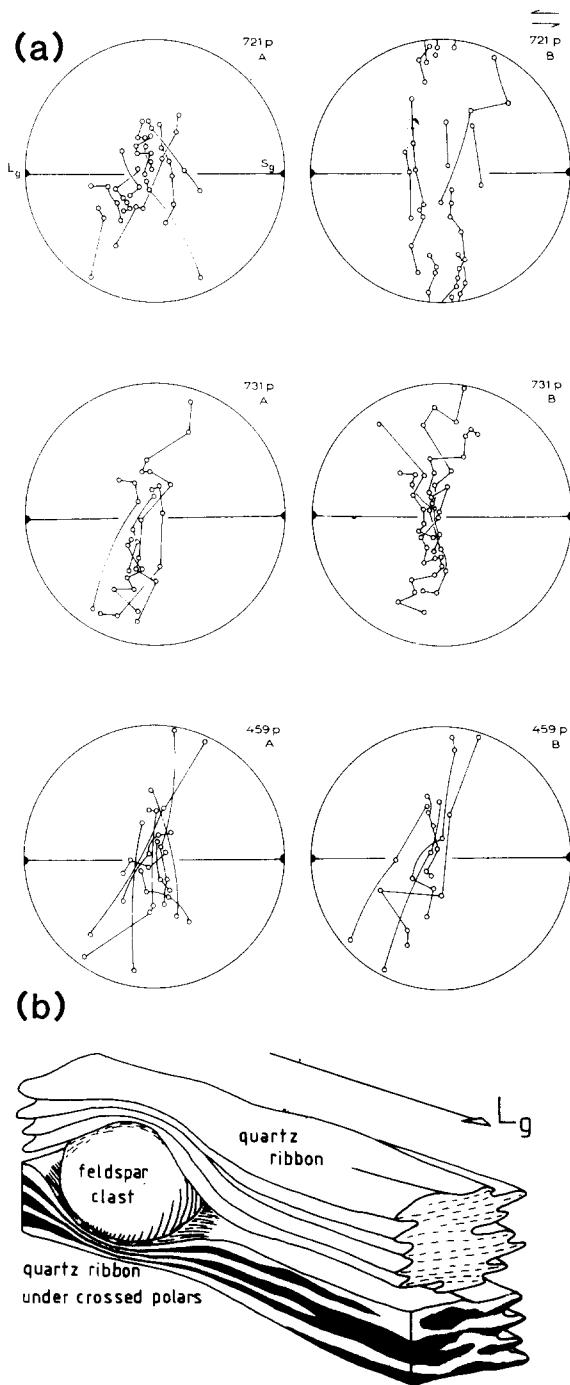


Fig. 5. a. Quartz *c*-axes traverse in quartz ribbons from three different samples. Lines connecting data points indicate the sequence of measurement on traverses normal to the long axes of the ribbons; data for each sample are spread over two plots for clarity.

b. Three-dimensional reconstruction of the quartz-ribbon microstructure.

wide and several centimetres long occur parallel to  $L_g$  in most samples of mylonitized granodiorite. Characteristic is a large length/width ratio (20–100) and a well-developed optical banding parallel to the ribbon's long axis, visible in thin sections parallel to  $L_g$  (Fig. 4; cf. Wilson, 1975; Bouchez, 1977; Boullier and Bouchez, 1978; Garcia-Celma, 1982). The orientation pattern of quartz *c*-axes changes gradually over each ribbon, defining a girdle normal to its long axis (Fig. 5a). This indicates that the quartz ribbons are tightly folded single crystals with fold axes parallel to the long axis of the ribbon and axial surfaces subparallel to  $S_g$  (Fig. 5b; cf. Marjoribanks, 1976; Bouchez, 1977; Garcia-Celma, 1982). Development of low- and high-angle grain boundaries in fold cores produced the characteristic banded aspect in sections parallel to  $L_g$ .

Quartz ribbons probably developed in response to dominant prism  $\langle a \rangle$  slip and minor basal slip (Bouchez, 1977). The presence of boudinaged rutile needles subparallel to the long axis of most ribbons indicates that little migration of high-angle grain boundaries took place; in all samples investigated local recrystallization led to destruction of the rutile needles. The ribbons probably developed from old grains favourably orientated for prismatic slip under conditions of effective recovery: at sites of enhanced strain rate, e.g. adjacent to feldspar porphyroclasts, recrystallization in the ribbons was more abundant (cf. Etheridge and Wilkie, 1979).

#### *Orthoclase*

Progressive intracrystalline deformation of orthoclase caused the development of undulose extinction, kink bands, deformation bands and microfaults, but was much less extensive than for quartz and micas (cf. Mitra, 1978). This is also indicated by the abundance of undeformed or weakly deformed inclusions of quartz or biotite in feldspar porphyroclasts. Dynamic recrystallization in response to high stored strain energy occurred in grain mantles (cf. Kerrick et al., 1980) and in micro-shear zones. The size of new grains shows little variation on a centimetre-scale and ranges from 1 to 5  $\mu\text{m}$  for all samples studied.

#### *Micro-shear zones in orthoclase*

Micro-shear zones occur as narrow zones of dynamically recrystallized feldspar transecting por-



Fig. 6. Extensional imbricate zone in a single orthoclase grain, with displacement along micro-shear zones. Crossed polars.



Fig. 8. Flame-shaped albite lamellae in perthitic orthoclase. Crossed polars.



Fig. 7. Detail of a micro-shear zone in orthoclase, consisting of fine-grained recrystallized feldspar and minor white mica. Crossed polars.

phyroclasts oblique to  $S_g$ , apparently uncontrolled by crystallographic directions (Fig. 6). At the boundary of these zones the lattice of the porphyroclast is sometimes bent, but there is no loss of cohesion (Fig. 7). Observations near the tip of partially developed zones indicate that growth occurred by nucleation of solitary new grains in narrow deformation bands. After sufficient new grains had nucleated and grown to impingement, the micro-shear zones acted as soft zones displacing relatively rigid porphyroclast fragments. With progressive deformation, the volume of recrystallized grains increased by widening of micro-shear zones and recrystallized mantles, finally producing rod- or disc-shaped domains of recrystallized material with few small porphyroclasts (Fig. 2; cf. Allison et al., 1979; Brown et al., 1980; Kerrick et al., 1980).

Nucleation of new feldspar grains seems to have taken place entirely by a classical nucleation mechanism (cf. Borges and White, 1980; Brown et al., 1980). No evidence for optical subgrain structures (Gorman, 1980; Vidal et al., 1980) or bulging of high-angle boundaries (Vernon, 1975) was observed.

#### *Flame-shaped perthite*

Besides common bead- or rod-shaped micro-perthitic lamellae, flame-shaped albite lamellae are common in weakly deformed porphyroclasts of orthoclase (Fig. 8). Flame-shaped lamellae are most common in grain mantles, near fractures, micro-shear zones and inclusions and generally in the most strongly deformed parts of a host crystal. The broadest part of the flame usually coincides with the area of most intense undulose extinction. In strongly deformed host grains the albite lamellae are commonly transected by faults or micro-shear zones. The lamellae formed during mylonitic deformation by exsolution of the albite component of orthoclase, up to 4 wt.% in the undeformed granodiorite (Passchier, 1982b). Strain-enhanced diffusion (White, 1975) probably aided the unmixing process.

#### *Plagioclase*

Intracrystalline deformation structures of plagioclase are very similar to those in orthoclase. Micro-shear zones are less common, and plagioclase porphyroclasts are usually less deformed and less recrystallized than orthoclase in any one sample.

Lenticular twins of the Albite and Pericline laws, considered to be deformation twins (cf. Vernon, 1965) are common, especially in kink and deformation bands.

#### *Feldspar transformation*

Fine, loboid myrmekite aggregates commonly replace oligoclase porphyroclasts along grain boundaries and micro-shear zones. Sericite grains, up to 10  $\mu\text{m}$  long grew in recrystallized aggregates of oligoclase and parallel to (001) or (010) cleavage traces in porphyroclasts. In plagioclase replacement by white mica is less common, mainly parallel to albite twins, along porphyroclast boundaries and in recrystallized aggregates. The total volume of replacement by micas is usually less than 5 vol.%. Microprobe analysis of feldspar porphyroclasts and recrystallized grains did not show any systematic difference in composition between old and new grains, in contrast with results by White (1975), Allison et al. (1979), Kerrick et al. (1980) and Vidal et al. (1980).

#### *Micas*

Biotite and muscovite were strongly deformed during mylonitic deformation. The crystals were either kinked and folded (Fig. 9) or boudinaged (Fig. 10), probably in response to the orientation of (001) planes in the shortening or extension field of the local incremental strain regime. Folded crystals are commonly kinked in the internal part of the fold arc accompanied by local dissolution (cf. Kerrick et al., 1980). Boudinaged grains have fractured at a



Fig. 9. Kinked biotite and folded muscovite in strongly mylonitized granodiorite.

low angle to (001). Dynamic recrystallization occurred mainly along grain mantles and kink band boundaries. New grains, 1–10  $\mu\text{m}$  in diameter, lack an obvious preferred orientation. Mica porphyroclasts are commonly lozenge-shaped, with a mean orientation of (001) oblique to  $S_g$ , dipping in opposite direction to the shear band cleavage. This probably reflects the relatively stable orientation of micas with (001) in the extension field of the incremental strain regime of mylonitic deformation. Deformation microstructures of biotite and muscovite are rather similar. Muscovite crystals are more commonly folded than kinked (Fig. 9) and fracturing along fold hinges or boudinage is more common than in biotite (cf. Wilson and Bell, 1979).

Biotite and muscovite porphyroclasts in the mylonitic granodiorite and mica megacrysts in the overlying undeformed granodiorite show small but systematic differences in chemical composition. Both biotite and muscovite clasts have higher FeO and  $\text{K}_2\text{O}$  values and lower  $\text{TiO}_2$ ,  $\text{Na}_2\text{O}$  and  $\text{Al}_2\text{O}_3$  values than in the undeformed granodiorite (Table 1). In addition biotite clasts have relatively low  $\text{SiO}_2$  and MgO values and muscovite clasts high  $\text{SiO}_2$  values (Table 1). In homogeneous metapelites, similar regional variations in mica composition are commonly attributed to differences in metamorphic grade (Miyashiro, 1973) and the observed variation in the granodiorite would correspond to a relatively low grade in the mylonitized section. Since the isograd pattern of Variscan metamorphism indicates an increase in metamorphic grade from granodiorite to basal gneiss (Passchier, 1982b; Vielzeuf, 1984), the observed variations cannot be attributed to the Variscan metamorphic gradient, but must be due to the later mylonitic deformation at retrograde conditions.

Recrystallization of biotite porphyroclasts was accompanied by a further depletion in  $\text{TiO}_2$  as indicated by a change in colour of the biotite and the presence of small ilmenite grains in aggregates of new grains (Fig. 9; cf. Kerrick et al., 1980). Locally biotite porphyroclasts were partly replaced by oligoclase (Passchier, 1982b). Advanced deformation of muscovite produced lozenge-shaped old grain relics mantled by a narrow rim of recrystallized white mica, invariably in a matrix of fine-grained biotite (Fig. 10). Major volumes of recrystallized white mica are absent, even where the original muscovite crystal was isolated, e.g. in a quartz domain.

TABLE 1

Representative compositions of primary muscovite (1–8) and biotite (1–7) in undeformed and mylonitized granodiorite

## (a) Muscovite

	Undeformed granodiorite			Mylonitized granodiorite					
	Mu 1	Mu 2	Mu 3	Mu 4	Mu 5	Mu 6	Mu 7	Mu 8	Mu 9
Na <sub>2</sub> O	0.51	0.47	0.41	0.36	0.41	0.35	0.38	0.29	0.47
MgO	0.56	0.52	0.79	0.58	0.69	0.63	0.61	0.70	0.64
Al <sub>2</sub> O <sub>3</sub>	35.68	35.38	36.16	35.47	35.62	35.24	34.99	35.90	35.74
SiO <sub>2</sub>	45.27	45.31	45.89	46.78	46.73	46.18	46.02	46.04	46.04
K <sub>2</sub> O	10.62	10.53	10.53	11.14	11.05	11.30	11.13	11.01	11.05
TiO <sub>2</sub>	1.58	1.62	1.41	0.43	0.73	n.m.	0.88	0.22	0.00
MnO	n.m.	n.m.	n.m.	0.01	0.05	n.m.	n.m.	0.03	0.01
FeO	0.97	0.71	0.99	0.66	0.93	1.47	1.07	0.92	1.77
Total	95.19	95.54	96.18	95.43	96.22	95.17	95.08	95.11	95.72

## (b) Biotite

	Undeformed granodiorite			Mylonitized granodiorite					
	Bi 1	Bi 2	Bi 3	Bi 4	Bi 5	Bi 6	Bi 7	Bi 8	Bi 9
Na <sub>2</sub> O	0.14	0.13	0.14	0.07	0.09	n.m.	n.m.	0.19	0.09
MgO	10.47	9.15	9.05	9.35	10.08	7.29	8.29	9.90	8.92
Al <sub>2</sub> O <sub>3</sub>	19.53	19.70	19.46	19.26	18.51	18.98	19.52	21.09	21.76
SiO <sub>2</sub>	35.43	35.06	34.92	35.22	36.12	34.45	34.92	36.71	34.98
K <sub>2</sub> O	9.62	9.57	9.42	9.81	9.95	9.92	9.67	9.33	9.84
TiO <sub>2</sub>	2.17	2.63	2.79	3.05	2.75	2.61	2.78	0.49	0.00
MnO	0.16	0.31	0.29	n.m.	0.21	0.19	0.27	0.09	0.16
FeO	17.26	18.90	18.68	19.44	17.74	23.18	21.28	18.08	19.65
Total	94.78	95.45	94.75	96.22	95.34	96.62	96.73	95.69	95.31

The Mu 9–Bi 9 pair was measured in the boudin neck of a sillimanite grain contained in a quartz megacryst. Bi 8 was measured in a new grain replacing recrystallized muscovite. The K<sub>2</sub>O contents appear to be somewhat low, particularly in Mu 2, resulting in only 80–95% filling of the X-positions. In biotite also the sums of the octahedrally coordinated cations are less than the ideal value (5.6 instead of 6.0). For analytical method see Appendix 1. n.m. – not measured.



Fig. 10. Fine-grained biotite replacing white mica along a micro-shear zone in a boudinaged muscovite porphyroblast.

### Sillimanite and accessory minerals

Sillimanite prisms and fibrolite aggregates were commonly boudinaged by fracturing normal to the long axis of the grains. This was accompanied by minor replacement by white mica and biotite in boudin necks (Fig. 11) even where sillimanite prisms are included in quartz megacrysts. The fine-grained muscovite replacing sillimanite or feldspar has a low TiO<sub>2</sub> and MnO content and is commonly overgrown by fine-grained biotite rich in Al<sub>2</sub>O<sub>3</sub> and with a low TiO<sub>2</sub> and MnO content (Table 1). Sillimanite breakdown is very incomplete.

Almandine, tourmaline, zircon and monazite reacted brittly to mylonitic deformation and frag-

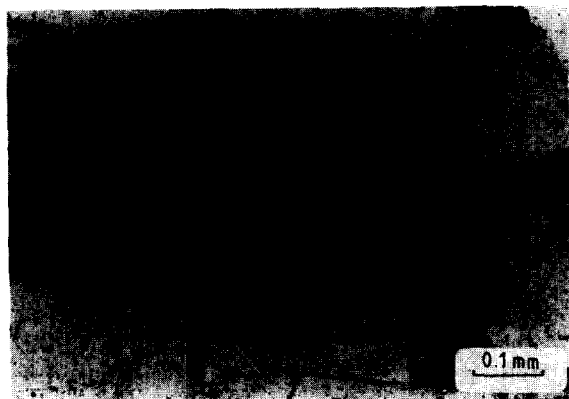


Fig. 11. Boudinaged sillimanite included in a major quartz grain. Fine-grained muscovite and biotite replace sillimanite at boudin necks.

ments remained stable throughout the deformation event (cf. White et al., 1980). Apatite recrystallized in a spectacular way from old equidimensional grains 1–2 mm in diameter to new polygonal, equidimensional grains 10–20  $\mu\text{m}$  in diameter in strongly flattened aggregates.

### Deformation in recrystallized aggregates

Grain boundary sliding and continuous recrystallization were probably the dominant deformation mechanisms in monomineralic and polymineralic aggregates of new feldspar and biotite grains (cf. Boullier and Gueguen, 1975; Schmid et al., 1977; Zeuch, 1983). This is indicated by the following data: (1) considerable displacement of feldspar porphyroblast fragments along micro-shear zones, up to 1 mm for a 10  $\mu\text{m}$  wide zone; (2) high aspect ratios of aggregates of new grains, up to 1000 : 1; (3) lack of optically detectable crystallographic preferred orientation in domains of new grains; (4) lack of change in internal microstructure, including grain size over major aggregates of new grains (Allison et al., 1979; Kerrick et al., 1980); (5) small size of new grains, below the limit of 10  $\mu\text{m}$  for grain boundary sliding for natural strain rates as proposed by Gorman (1980); and (6) a polymineralic aspect of most aggregates.

Quartz ribbons and rod-shaped aggregates of recrystallized feldspar with porphyroblast fragments commonly have similar length/width ratios in the mylonite, although intracrystalline ductile deforma-

tion of quartz was much more effective than that of feldspar. This apparent contradiction can be explained by the relatively low yield strength of material deforming by grain boundary sliding (Allison et al., 1979; Kerrick et al., 1980). Even if feldspar porphyroclasts would act as perfectly rigid bodies, feldspar domains could still deform at equal rate as quartz domains if strain in the former was taken up by the generation of micro-shear zones and grain boundary sliding in the recrystallized material. In some samples, quartz ribbons display brittle fractures which do not continue into the surrounding aggregates of recrystallized feldspar. This suggests that in late stages of mylonitic deformation the strain rate of grain boundary sliding in the aggregates could not be accommodated by crystal plastic deformation of quartz, leading to brittle fracturing.

### Metamorphic conditions

The granodioritic parent rock of the mylonites described above reached upper amphibolite facies peak metamorphic conditions as indicated by the stable coexistence of quartz-plagioclase ( $\text{An}_{10-30}$ )-orthoclase-biotite-sillimanite-cordierite-almandine in granodiorite, of forsterite-diopside-grossular-plagioclase-calcite in calcsilicate lenses in the granodiorite and of green hornblende, plagioclase ( $\text{An}_{50-70}$ )-biotite-quartz and quartz, plagioclase-diopside in metabasite lenses. Vielzeuf (1984) postulates peak metamorphic conditions of 650–750°C and 400–500 MPa in the top of the basal gneiss. From these conditions, a retrogressive path has been followed in the granodiorite up to the onset of mylonitic deformation. This is indicated by the late growth of large, euhedral muscovite over orthoclase, plagioclase, biotite and sillimanite and by replacement of garnet by biotite and cordierite. Fe-Mg partitioning between coexisting late biotite or cordierite and almandine indicate temperatures of 530–620°C (Passchier, 1982b; Vielzeuf, 1984). In calcsilicate and metabasite lenses plagioclase is partly replaced by scapolite; hornblende and diopside partly by epidote, clinozoisite, cummingtonite and actinolite (Zwart, 1954; Passchier, 1982b).

During mylonitic deformation, *P-T* conditions had fallen even further as indicated by: (1) stable mineral paragenesis in deformed granodiorite of plagioclase ( $\text{An}_{0-20}$ )-almandine-biotite-muscovite-ilmenite; and (2) the compositional variations of

biotite and muscovite between deformed and undeformed granodiorite. Combined with data from fluid inclusion densities in deformed quartz grains and crystallographic *c*-axis fabrics of quartz, this indicates conditions of 450–550°C and 200–300 MPa (mean stress) during at least the last part of the mylonitic event (Passchier, 1982b, 1983, 1984b). The development of late pseudotachylytic and ultramylonitic shear-bands in the mylonite zone, and a systematic change from quartz fabric patterns corresponding to prism *a* slip to basal slip (Passchier, 1982a, 1982b, 1983) probably result from falling *P-T* conditions during the mylonitic event (cf. Boullier and Bouchez, 1978; Simpson et al., 1982).

Mylonitization in granodiorite of the Saint-Barthélemy Massif affected all mineral phases by grain size reduction (cf. Etheridge and Wilkie, 1979; White et al., 1980) but the mineralogical and chemical changes involved are of minor importance. Systematic changes in chemical composition of con-

stituent minerals involve slight alterations in composition of biotite and muscovite porphyroclasts, TiO<sub>2</sub> and MnO loss from recrystallized biotite and unmixing of orthoclase to produce perthite. The most important mineral reactions observed are shown in Fig. 12. They are expressed for mineral pairs since they are usually observed in originally monomineralic domains. These reactions are all very incomplete and affect only a few percent of the parent minerals involved. Exact percentages cannot be estimated due to the heterogeneity of the rock and the fine-grained nature of the recrystallized material. As shown in Fig. 12, the sum of ion exchanges between the reactions can add up to an isochemical total with the exception of the necessary introduction of water and minor MgO, FeO and TiO<sub>2</sub>. The change in chemical composition of mica porphyroclasts does not necessarily violate isochemical behaviour of the rock since it may have been accommodated by re-equilibration of garnet composition,

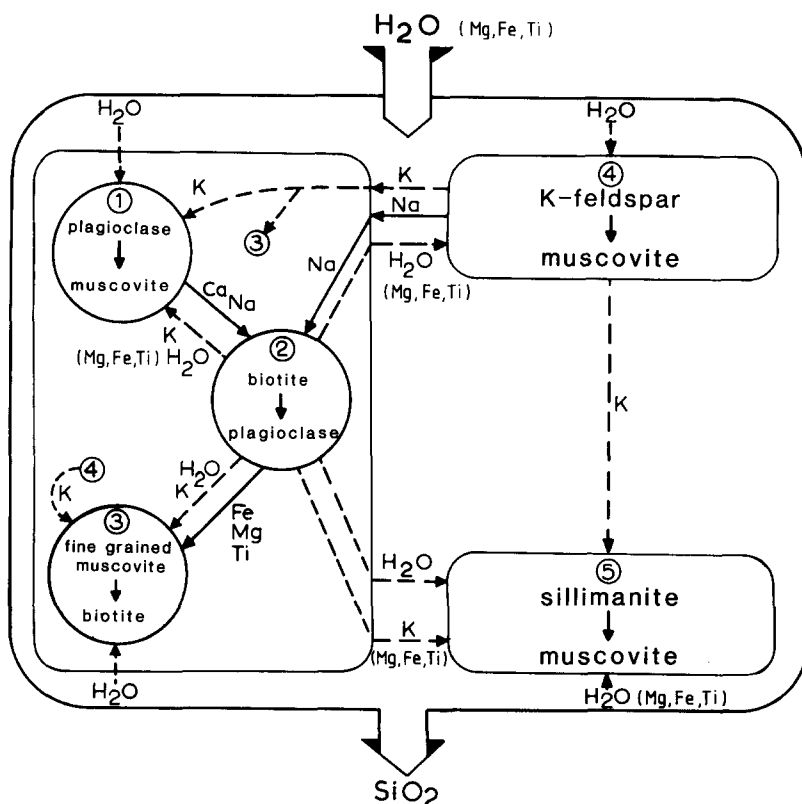
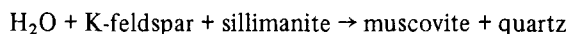


Fig. 12. Schematic representation of the reactions observed in mylonitized granodiorite. Necessary paths of material exchange in solid arrows, possible paths in dotted arrows. Exchange of SiO<sub>2</sub> between reactions has been omitted since quartz is present in excess. Details are given in the text and in Appendix 2.

ilmenite growth and replacement of sillimanite and orthoclase by muscovite (Fig. 12). The large width of the ductile shear zone and inhomogeneity of the parent granodiorite do not allow further assessment of possible isochemical behaviour.

## Discussion

The reactions observed can be split into a self-contained group *A* (Fig. 12) with little effect on the mineral assemblage of the rock and a reaction pair *B* representing the retrograde transformation:



The reactions of group *A* can be explained as being "mechanically" driven by the mylonitic deformation. Reaction (1) (see Appendix 2) would produce a volume decrease of the solid phases involved while reactions (2) and (3) produce a proportional volume increase (Beach, 1979). In fact reaction (3) is mainly observed in boudin necks of white mica and sillimanite grains (Figs. 10 and 11) and in pressure shadow domains of large feldspar grains, i.e. in those areas which favour a volume increase. Gradients of normal stresses with a short wavelength, which are likely to be set up by incremental strains in a heterogeneous mylonite, could drive each of the reactions of group *A* in neighbouring domains with short-range ion exchange (Fry, 1982). Further deformation would tend to shift active transformation to new domains following changes in the stress gradients. In an actively deforming material continuous distortion of chemical gradients will affect the progress of reactions as well.

### *Water-deficient conditions*

Since mylonitic deformation is thought to enhance diffusion (White et al., 1980), the incompleteness of the retrograde reactions of Fig. 12 is unusual. Analysis of the fluid inclusion content in quartz grains in the mylonite yielded pure CO<sub>2</sub> in all cases (Passchier, 1982b, 1984b). A low water content of the metamorphic fluid during the deformation explains these data best. Sillimanite and orthoclase provide a buffer of progressively lower  $P_{\text{H}_2\text{O}}$  as the rock cools into the stability field of muscovite + quartz as defined for  $P_{\text{H}_2\text{O}} = P_{\text{total}}$  (Kerrick, 1972; Yardley, 1980). The influx of aqueous fluids will

have determined the rate at which these reactions could proceed, but was in most cases insufficient to destroy the buffer. Local progress of one of the reactions of group *A* (Fig. 12), involving hydrous-anhydrous mineral pairs, could accelerate or slow the progress of sillimanite-orthoclase breakdown in the same domain by a complex redistribution of the available water. The limited availability of aqueous fluids may be due to an increased geothermal gradient and upward migrating CO<sub>2</sub>-rich fluids along the mylonite zone, interpreted as a low-angle normal fault zone over a basement of mainly granulitic gneisses (Passchier, 1984c).

### *Differential stress*

Pseudotachylyte veins were generated in the granodiorite at a late stage of mylonitic deformation, and many such veins underwent ductile deformation to ultramylonite (Passchier, 1982a, 1984a). Ductile reactivation of pseudotachylyte is a rare phenomenon and may be due to relatively high metamorphic conditions of pseudotachylyte generation (Passchier, 1982a, 1984a). This effect, and brittle fracturing of quartz ribbons in some granodiorite samples probably reflect unusually high differential stresses for local *P-T* and strain rate values, exceeding the brittle shear strength of the material.

Grain size of dynamically recrystallized quartz (7–30 μm) and feldspar (1–5 μm) in the mylonitized granodiorite have a similar ratio as observed in other mylonite zones (cf. Christie and Ord, 1980; Etheridge and Wilkie, 1981). The size of dynamically recrystallized grains, unaffected by static grain growth, depends on the magnitude of the contemporary differential stress (Christie and Ord, 1980). Grain sizes observed for quartz correspond to values of 50–110 MPa during mylonitic deformation. This is relatively high compared with values from other mylonite zones in granitoid material formed at similar metamorphic conditions (Etheridge and Wilkie, 1981). It can be an effect of limited hydrolytic weakening due to a low water content of the metamorphic fluid, buffered by retrograde reactions (Tullis and Yund, 1980; Yardley, 1980).

### *Postkinematic grain growth*

Although the microfabric described above is

characteristic for most of the mylonitized granodiorite, significant deviations occur in isolated outcrops with identical macrofabric and orientation of shape fabric elements as elsewhere in the ductile shear zone. In mylonite from these outcrops, pseudotachylyte veins are lacking and the retrograde reactions described above have proceeded much further. Recrystallized grains of quartz and feldspar show undulose extinction and the development of new subgrains, but their size exceeds the ranges stated above since they have been affected by postkinematic grain boundary migration (Fig. 3; cf. White, 1976). In some samples postkinematic grain growth produced aggregates of large strain-free new grains of polygonal quartz and feldspar and hypidiomorphic biotite and white mica. In those samples the retrograde reactions of Fig. 12 have gone nearly to completion, chlorite and epidote are additional new mineral phases and aqueous fluid inclusions are present in quartz grains. A locally high water content of the metamorphic fluid during mylonite deformation can explain the development of these deviant fabrics. Apparently, a low water content of the metamorphic fluid hampered postkinematic grain growth of quartz, feldspar and micas alike in most of the mylonite zones.

### Recognition of water-deficient mylonite zones

The water-deficient nature of the low-grade mylonite zone in the Saint-Barthélemy Massif can be attributed to a small proportion of hydrous minerals, a relatively large volume of metastable sillimanite and orthoclase and small influx of aqueous fluids.

In many samples from the mylonite zone, sillimanite, orthoclase and almandine appear to be part of a stable synkinematic paragenesis, and retrograde reactions are easily missed. Since this might cause misinterpretation of deformation conditions, a number of criteria should be defined to recognize water-deficient mylonite zones.

From observations in the Saint-Barthélemy Massif, the most reliable criteria for the recognition of water-deficient mylonite zones seem to be: (1) fluid inclusions with a limited water content; (2) relative importance of retrograde reactions which are little dependent on water influx, e.g. exsolution of albite from orthoclase; (3) small importance of water

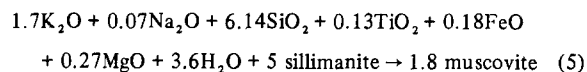
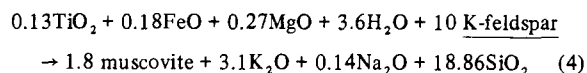
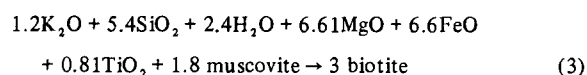
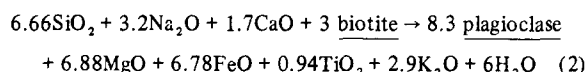
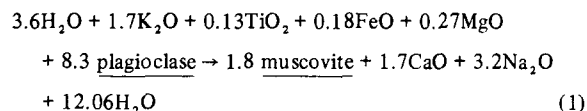
consuming retrograde reactions; (4) the presence of ductilely deformed pseudotachylyte veins and small size of dynamically recrystallized grains, representing relatively high differential stresses; and (5) limited static recrystallization. The recognition of local zones where retrograde reactions were more complete and postkinematic grain growth occurred, combined with analysis of fluid inclusion density can help to define actual deformation conditions.

### Appendix 1 – Analytical method

Mineral analyses have been carried out with Cambridge Geoscan and microscan Mark-9 electron microprobe instruments. General operating conditions were 20 kV accelerating potential, 25 nA sample current. Standards used include Diopside for Si and Ca, Olivine for Mg, Jadeite and Albite for Na, Orthoclase for K, Corundum for Al, Hematite for Fe, Almandine for Al, Si and Fe, Rhodonite for Mu and synthetic TiO<sub>2</sub> for Ti. A LINK system was used for semi-quantitative analyses.

### Appendix 2

The reactions shown in Fig. 12 are:



Reactions (1)–(3) are balanced for constant Al. Composition used in the reactions are:

Plagioclase – Na<sub>0.8</sub>Ca<sub>0.2</sub>Al<sub>1.2</sub>Si<sub>2.8</sub>O<sub>8</sub> (optically determined)

K-feldspar – K<sub>0.96</sub>Na<sub>0.04</sub>AlSi<sub>3</sub>O<sub>8</sub> (K/Na ratio by microprobe)

Sillimanite – Al<sub>2</sub>SiO<sub>5</sub>

Quartz – SiO<sub>2</sub>

Muscovite – K<sub>1.89</sub>Na<sub>0.07</sub>Al<sub>3.73</sub>Ti<sub>0.07</sub>Fe<sub>0.10</sub>Mg<sub>0.15</sub>Si<sub>6.19</sub>Al<sub>1.81</sub>O<sub>20</sub>(OH)<sub>4</sub> (Table 1 – Mu 4)

Biotite – Na<sub>0.03</sub>K<sub>1.92</sub>Mg<sub>2.27</sub>Fe<sub>2.24</sub>Ti<sub>0.31</sub>Al<sub>3.30</sub>Si<sub>5.46</sub>O<sub>20</sub>(OH)<sub>4</sub> (Table 1 – Bi 5)

## References

- Allison, J., Barnett, R.L. and Kerrick, R., 1979. Superplastic flow and changes in crystal chemistry of feldspars. *Tectonophysics*, 53: T41–T46.
- Beach, A., 1976. The interrelations of fluid transport, deformation, geochemistry and heat flow in early Proterozoic shear zones in the Lewisian complex. *Philos. Trans. R. Soc. London, Ser. A*, 280: 569–604.
- Beach, A., 1979. Pressure solution as a metamorphic process in deformed terrigenous sedimentary rocks. *Lithos*, 12: 51–58.
- Borges, F.S. and White, S.H., 1980. Microstructures and chemical studies of sheared anorthosites. *J. Struct. Geol.*, 2: 273–280.
- Bouchez, J.L., 1977. Plastic deformation of quartzites at low temperature in an area of natural strain gradient. *Tectonophysics*, 39: 25–30.
- Boullier, A.M. and Bouchez, J.L., 1978. Le quartz en rubans dans les mylonites. *Bull. Soc. Géol. Fr.*, 20: 253–262.
- Boullier, A.M. and Gueguen, Y., 1975. SP-mylonites: origin of some mylonites by superplastic flow. *Contrib. Mineral. Petrol.*, 50: 93–104.
- Brodie, K.H., 1981. Variation in amphibole and plagioclase composition with deformation. *Tectonophysics*, 78: 385–402.
- Brown, W.L., Macaudiere, J. and Ohnenstetter, M., 1980. Ductile shear zones in a meta-anorthosite from Harris, Scotland: textural and compositional changes in plagioclase. *J. Struct. Geol.*, 2: 281–287.
- Burwash, R.A. and Krupicka, J., 1969. Cratonic reactivation in the Precambrian basement of Western Canada, I. Deformation and chemistry. *Can. J. Earth Sci.*, 6: 1381–1396.
- Christie, J.M. and Ord, A., 1980. Flow stress from microstructures of mylonites: example and current assessment. *J. Geophys. Res.*, 85-B11: 6253–6262.
- Etheridge, M.A. and Wilkie, J.C., 1979. Grain size reduction, grain boundary sliding and the flow strength of mylonites. *Tectonophysics*, 58: 159–178.
- Etheridge, M.A. and Wilkie, J.C., 1981. An assessment of dynamically recrystallized grain size as a palaeopiezometer in quartz-bearing mylonite zones. *Tectonophysics*, 78: 475–508.
- Fry, N., 1982. Metamorphic incongruent solution, diffusion and pressure solution stripes. *Lithos*, 15: 183–190.
- García Celma, A., 1982. Domainal and fabric heterogeneities in the Cap de Creus quartz mylonites. *J. Struct. Geol.*, 4: 443–457.
- Gorman, B.E., 1980. A model of flow and fracture in plagioclase: examples from shear zones, Fiskenaeset complex, west Greenland. Ph.D. Thesis, University of Toronto, Toronto, Ont. (unpublished).
- Kerrick, D.M., 1972. Experimental determination of muscovite + quartz stability with  $P(\text{H}_2\text{O}) < P(\text{total})$ . *Am. J. Sci.*, 272: 946–958.
- Kerrick, R., Allison, J., Barnett, R.L., Moss, S. and Starkey, J., 1980. Microstructural and chemical transformations accompanying deformation of granite in a shear zone at Mieville, Switzerland. *Contrib. Mineral. Petrol.*, 73: 221–243.
- Lister, G.S. and Williams, P.F., 1983. The partitioning of deformation in flowing rock masses. *Tectonophysics*, 92: 1–33.
- Marjoribanks, R.W., 1976. The relation between microfabric and strain in a progressively deformed quartzite sequence from central Australia. *Tectonophysics*, 32: 269–293.
- McCaig, A.M. and Wickham, S.M., 1984. The tectonic evolution of the Pyrenees: A workshop. *J. Geol. Soc. London*, 141: 379–381.
- Mitra, G., 1978. Ductile deformation zones and mylonites. *Am. J. Sci.*, 278: 1057–1084.
- Passchier, C.W., 1982a. Pseudotachylyte and the development of ultramylonite bands in the Saint-Barthélemy Massif, French Pyrenees. *J. Struct. Geol.*, 4: 69–79.
- Passchier, C.W., 1982b. Mylonitic deformation in the Saint-Barthélemy Massif, French Pyrenees. *G.U.A. Pap. Geol.*, 1(16), 173 pp.
- Passchier, C.W., 1983. The reliability of asymmetric *c*-axis fabrics of quartz to determine sense of vorticity. *Tectonophysics*, 99: T9–T18.
- Passchier, C.W., 1984a. The generation of ductile and brittle shear bands along a low-angle mylonite zone, French Pyrenees. *J. Struct. Geol.*, 6: 273–281.
- Passchier, C.W., 1984b. Fluid inclusions in pseudotachylyte and ultramylonite. *Bull. Minéral.*, 107: 307–315.
- Passchier, C.W., 1984c. Mylonite-dominated footwall geometry – an example from the Pyrenees. *Geol. Mag.*, 121: 429–436.
- Ramsay, J.G. and Allison, J., 1979. Structural analysis of shear zones in an alpinised Hercynian granite. *Schweiz. Mineral. Petrogr. Mitt.*, 59: 251–279.
- Schmid, S.M., Boland, J.N. and Paterson, M.S., 1977. Superplastic flow in fine-grained limestone. *Tectonophysics*, 43: 257–291.
- Simpson, C. and Schmid, S.M., 1983. An evaluation of criteria to deduce sense of movement in sheared rocks. *Bull. Geol. Soc. Am.*, 94: 1281–1288.
- Simpson, C., Carreras, J. and Losantos, M., 1982. Inhomogeneous deformation in Roses granodiorite, N.E. Spain. *Acta Geol. Hisp.*, 17: 219–226.
- Tullis, J. and Yund, R.A., 1980. Hydrolytic weakening of experimentally deformed Westerly granite and Hale albite rock. *J. Struct. Geol.*, 2: 439–451.
- Vernon, R.H., 1965. Plagioclase twins in some mafic gneisses from Broken Hill, Australia. *Mineral. Mag.*, 35: 488–507.
- Vernon, R.H., 1975. Natural deformation and recrystallization of a plagioclase grain. *Am. Mineral.*, 60: 884–888.
- Vidal, J.L., Kubin, L., Debat, P. and Soula, J.C., 1980. Deformation and dynamic recrystallization of K-feldspar augen in orthogneiss from Montagne Noire, Occitania. *Lithos*, 13: 247–257.
- Vielzeuf, D., 1984. Relations de phases dans le faciès granulite et implications géodynamiques. L'exemple des Pyrénées. Ph.D. Thesis, University of Clermont-Ferrand, Clermont-Ferrand (unpublished).
- White, S., 1975. Tectonic deformation and recrystallization of oligoclase. *Contrib. Mineral. Petrol.*, 50: 287–305.

- White, S., 1976. The role of dislocation processes during tectonic deformation with particular reference to quartz. In: R.J. Strens (Editor), *The Physics and Chemistry of Minerals and Rocks*, Wiley-Interscience, London, pp. 75–91.
- White, S., Burrows, S.E., Carreras, J., Shaw, N.D. and Humphreys, F.J., 1980. On mylonites in ductile shear zones. *J. Struct. Geol.*, 2: 175–187.
- Wilson, C.J.L., 1975. Preferred orientation in quartz ribbon mylonites. *Bull. Geol. Soc. Am.*, 86: 968–974.
- Wilson, C.J.L. and Bell, J.A., 1979. Deformation of biotite and muscovite: optical microstructure. *Tectonophysics*, 58: 179–200.
- Yardley, B.W.D., 1980. Effect of cooling on the water content and mechanical behaviour of metamorphosed rocks. *Geology*, 9: 151–408.
- Zeuch, D., 1983. On the interrelationship between grain size sensitive creep and dynamic recrystallization of olivine. *Tectonophysics*, 93: 151–168.